Solid-State Nuclear Magnetic Resonance Measurements of HIV Fusion Peptide to Lipid Distances Reveal the Intimate Contact of β Strand Peptide with Membranes and the Proximity of the Ala-14−Gly-16 Region with Lipid Headgroups†

Wei Qiang,‡ Jun Yang,§ and David P. Weliky*,‡

Department of Chemistry, Michigan State University, East Lansing, Michigan 48824, and Department of Molecular Cardiology, Lerner Research Institute, Cleveland Clinic Foundation, Cleveland, Ohio 44195

Received December 1, 2006; Revised Manuscript Received February 23, 2007

ABSTRACT: Human immunodeficiency virus (HIV) infection begins with fusion between viral and host cell membranes and is catalyzed by the HIV gp41 fusion protein. The ∼20 N-terminal apolar residues of gp41 are called the HIV fusion peptide (HFP), interact with the host cell membrane, and play a key role in fusion. In this study, the membrane location of peptides which contained the HFP sequence (AVGIGALFLGFLGAAGSTMGARS) was probed in samples containing either only phospholipids or phospholipids and cholesterol. Four HFPs were examined which each contained ^{13}CO labeling at three sequential residues between G5 and G16. The ^{13}CO chemical shifts indicated that HFP had predominant β strand conformation over the labeled residues in the samples. The internuclear distances between the HFP ^{13}CO groups and the lipid ^{31}P atoms were measured using solid-state nuclear magnetic resonance rotational-echo double-resonance experiments. The shortest ^{13}CO−^{31}P distances of 5−6 Å were observed for HFP labeled between A14 and G16 and correlated with intimate association of β strand HFP and membranes. These results were confirmed with measurements using HFPs singly labeled with ^{13}CO at A6 or A14. To our knowledge, these data are the first measurements of distances between HIV fusion peptide nuclei and lipid P, and qualitative models of the membrane location of oligomeric β strand HFP which are consistent with the experimental data are presented. Observation of intimate contact between β strand HFP and membranes provides a rationale for further investigation of the relationship between structure and fusion activity for this conformation.

The infection of enveloped viruses such as human immunodeficiency virus (HIV)[1] begins with fusion between the viral and host cell membranes (*1*−*4*). Fusion may be catalyzed by fusion proteins, and several models of fusion protein catalysis have been proposed (*2*, *5*−*7*). For HIV, fusion is catalyzed by a "gp160" glycoprotein complex which is incorporated in the virus membrane and is composed of two noncovalently associated subunits, "gp120" and "gp41". The gp120 subunit lies outside the virus and binds to receptors in the target cell membrane, and the gp41 subunit contains a region inside HIV as well as a single-pass transmembrane domain (*8*, *9*). The ∼170-residue ectodomain of gp41 lies outside HIV and is subdivided into a more C-terminal "soluble ectodomain" and an ∼20-residue N-terminal fusion peptide (HFP) which is apolar and fairly conserved. The HFP is believed to interact with the target cell membrane after gp120 binds to cellular receptors, and fusion is greatly disrupted by mutation or deletion of the HFP (*10*−*13*).

Peptides with the HFP sequence catalyze vesicle fusion, and there are good correlations between the mutation−fusion activity relationships of HFP-induced vesicle fusion and HIV−target cell fusion (*14*−*17*). Studies of membrane-associated HFP should therefore provide useful information about some aspects of biological fusion. Both the conformation and membrane location of the HFP have been hypothesized to be significant structural factors for the catalysis of fusion by the HFP (*16*, *18*). The conformation of the HFP has been investigated in detergent micelles and membranes using a variety of biophysical techniques. For HFP associated

† This work was supported by NIH Grant AI47153 to D.P.W.

* To whom correspondence should be addressed. Telephone: (517) 355-9715. Fax: (517) 353-1793. E-mail: weliky@chemistry.msu.edu.

‡ Michigan State University.

§ Cleveland Clinic Foundation.

[1] Abbreviations: ^{14}AAG, residues A14, A15, and G16; ^{13}CO, ^{13}C-labeled carbonyl; *d*, magnitude of ^{13}C−^{31}P dipolar coupling; DPPC-^{13}C, 1,2-dipalmitoyl-*sn*-glycero-3-phosphocholine with ^{13}C labeling at both carbonyl sites; DTPC, 1,2-di-*O*-tetradecyl-*sn*-glycero-3-phosphocholine; DTPG, 1,2-di-*O*-tetradecyl-*sn*-glycero-3-[phospho-*rac*-(1-glycerol)]; *f*, fraction of ^{13}CO groups close to ^{31}P atoms; FMI, full membrane insertion; ^{5}GALFLGFLG, residues G5, A6, L7, F8, L9, G10, F11, L12, and G13; HEPES, *N*-(2-hydroxyethyl)piperazine-*N*′-2-ethanesulfonic acid; HFP, HIV fusion peptide; HFP1, AVGIGALFLGFLGAAGSTMGARS-NH_2; HFP1-^{8}FLG, HFP1 labeled with ^{13}CO at F8, L9, and G10; HFP2, AVGIGALFLGFLGAAGSTMGARSKKK-NH_2; HFP2-^{5}GAL, HFP2 labeled with ^{13}CO at G5, A6, and L7; HFP2-^{11}FLG, HFP2 labeled with ^{13}CO at F11, L12, and G13; HFP2-^{14}AAG, HFP2 labeled with ^{13}CO at A14, A15, and G16; HFP3, AVGIGALFLGFLGAAGSTMGARSKKKA$_\beta$; HFP3-^{8}FLG, HFP3 labeled with ^{13}CO at F8, L9, and G10; HFP4, AVGIGALFLGFLGAAGSTMGARSWKKKKKKA$_\beta$; HFP4-^{6}A, HFP4 labeled with ^{13}CO at A6; HFP4-^{14}A, HFP4 labeled with ^{13}CO at A14; HIV, human immunodeficiency virus; IR, infrared; ^{7}LFLGFL, residues L7, F8, L9, G10, F11, and L12; MAS, magic angle spinning; NMR, nuclear magnetic resonance; PC:PG, 4:1 DTPC/DTPG mixture; PC:PG:CHOL, 8:2:5 DTPC/DTPG/cholesterol mixture; PMI, partial membrane insertion; *r*, ^{13}C−^{31}P internuclear distance; REDOR, rotational-echo double-resonance; τ, duration of the dephasing period; TFA, trifluoroacetic acid.

10.1021/bi6024808 CCC: $37.00
Published on Web 04/07/2007

with negatively charged sodium dodecyl sulfate micelles, one liquid-state nuclear magnetic resonance (NMR) study showed that there was uninterrupted α helical structure from I4 to M19, while another study showed a helix from I4 to A14 followed by a β turn (*19*, *20*). For HFP associated with neutral dodecylphosphocholine micelles, helical structure was detected from I4 to L12 (*21*; C. M. Gabrys and D. P. Weliky, unpublished data). There is not yet a consensus for the micelle location of HFP, and there are distinct models based on experiment and simulation of either predominant micelle surface location or micelle traversal by HFP (*19*−*23*). In one NMR study, residues I4−A15 were found to be fully shielded from solvent and residues G3 and G16 were at the micelle−solvent interface (*20*).

The conformation of membrane-associated HFP has been investigated with different lipid components and different peptide:lipid ratios. A greater fraction of HFPs adopted helical structure at low peptide:lipid ratios, while nonhelical structure became more favored at higher ratios (*24*). Helical structure was also promoted by negatively charged lipids, while a higher fraction of β strand structure was adopted with neutral lipids or with bound Ca^{2+} (*16*, *24*−*26*). Solid-state NMR provided residue-specific conformational information about HFP associated with membranes whose lipid headgroup and cholesterol composition were comparable to those of host cells of the virus. A β strand conformation was observed for residues A1−G16, while A21 appeared to be unstructured (*27*, *28*). Formation of β strand oligomers or aggregates was supported by detection of short distances between labeled ^{13}CO groups on one HFP and labeled ^{15}N on an adjacent HFP (*29*). Oligomerization and aggregation have also been detected by other biophysical methods (*15*, *30*). There is evidence that at least the lipid mixing step of membrane fusion can occur with the HFP in either helical or β strand conformation, although there is some controversy in the literature about this conclusion (*14*, *16*, *18*, *31*−*35*).

HFP location in membranes has been primarily probed using an HFP-F8W mutant and by variation of the tryptophan fluorescence of this mutant with changes in environment (*36*, *37*). Key results have included the following. (1) Fluorescence was higher for membrane-associated HFP-F8W than for HFP-F8W in a buffered saline solution. (2) Greater fluorescence quenching by acrylamide was observed for a soluble tryptophan analogue than for membrane-associated HFP-F8W. (3) Similar fluorescence quenching of membrane-associated HFP-F8W was observed in samples containing either 1-palmitoyl-2-stearoylphosphocholine brominated at the 6 and 7 carbons of the stearoyl chain or the corresponding lipid brominated at the 11 and 12 carbons of the chain. The first two results indicated that the level of solvent exposure of the HFP-F8W tryptophan is reduced with membrane association, and the third result indicated that the membrane location of the tryptophan indole group is centered near the carbon 9 position of the brominated lipid stearoyl chain, i.e., ∼8.5 Å from the bilayer center and ∼10 Å from the lipid phosphorus. Infrared (IR) and solid-state NMR spectra of membrane-associated HFP suggested that HFP-F8W had predominant β strand conformation under the conditions of the fluorescence experiments (*16*, *27*, *36*, *37*).

In a different set of experiments, electron spin resonance spectra showed that chromium oxalate in the aqueous phase quenched the signal of membrane-associated HFP which was spin-labeled at M19 but did not quench HFP spin-labeled at A1 (*30*). These data indicated a location for M19 close to the aqueous interface of the membrane and a location for A1 away from this interface.

Models for HFP location in membranes have also been developed from simulations of a single HFP molecule in membranes and have shown either partial insertion or traversal of the membrane. The HFP always adopted predominant α helical conformation and in one simulation was generally near the membrane surface with the F8 backbone and side chain nuclei 4 and 6 Å deeper than the phosphorus longitude, respectively (*38*). For a different simulation, HFP traversed the membrane and the backbone and side chain F8 nuclei were at the bilayer center, i.e., ∼19 Å from the phosphorus longitude (*39*).

This paper includes solid-state NMR measurements of distances between ^{13}C-labeled carbonyl (^{13}CO) nuclei in HFP and lipid ^{31}P nuclei. These studies provide information about the location of specific HFP residues relative to the phosphorus headgroups and are complementary to other solid-state NMR methods of probing membrane location of peptides and proteins (*40*−*50*). The $^{13}CO-^{31}P$ distance approach has previously been used to probe the locations of antimicrobial peptides, antibiotics, and sterols in membranes (*51*−*53*). Measurements were taken both on HFP associated with membranes containing only phospholipids and on HFP associated with membranes which contained both phospholipids and cholesterol. The potential significance of cholesterol-containing membranes is suggested both by the cholesterol:phospholipid molar ratios of ∼0.5 and 0.8 for HIV host cell and HIV membranes, respectively, and by the observation that β strand conformation of HFP is promoted by membrane cholesterol (*27*, *35*, *54*−*57*).

The $^{13}CO-^{31}P$ distances (r) were probed with the rotational-echo double-resonance (REDOR) technique which is a solid-state NMR method for measuring magnitudes of dipolar couplings (d) between spin $^1/_2$ heteronuclei such as ^{13}C and ^{31}P (*58*). For a $^{13}CO-^{31}P$ spin pair, $r = 23.05/d^{1/3}$, where r and d are in units of angstroms and hertz, respectively. The upper limit of REDOR detection of r is ∼10 Å ($d \geq 10$ Hz) (*35*).

MATERIALS AND METHODS

Materials. Resins and 9-fluorenylmethoxycarbonyl (FMOC) amino acids were obtained from Peptides International (Louisville, KY). Amino acids isotopically labeled with ^{13}CO were obtained from Cambridge Isotope Laboratories (Andover, MA). The lipids 1,2-di-*O*-tetradecyl-*sn*-glycero-3-phosphocholine (DTPC), 1,2-di-*O*-tetradecyl-*sn*-glycero-3-[phospho-*rac*-(1-glycerol)] (DTPG), and [1-^{13}C]-1,2-dipalmitoyl-*sn*-glycero-3-phosphocholine (DPPC-^{13}C) were obtained from Avanti Polar Lipids (Alabaster, AL). The 5 mM HEPES buffer at pH 7 contained 0.01% (w/v) NaN_3 preservative.

Peptides. All peptides contained the sequence AVGIGALFLGFLGAAGSTMGARS which is the 23 N-terminal residues of HIV-1 gp41, LAV_{1a} strain. A set of peptides for probing peptide−lipid headgroup distances between G5 and G16 were synthesized. "HFP1-^{8}FLG" had the sequence AVGIGALFLGFLGAAGSTMGARS-NH_2 and was labeled with ^{13}CO at F8, L9, and G10. "HFP2-^{5}GAL", "HFP2-^{11}-

FLG", and "HFP2-^{14}AAG" had the sequence AVGIGALFLG-FLGAAGSTMGARSKKK-NH_2 and were labeled with ^{13}CO at G5, A6, and L7, at F11, L12, and G13, and at A14, A15, and G16, respectively. The three non-native lysines increased the aqueous solubility and resulted in monomeric peptide in the buffer solution prior to membrane binding (*59*). "HFP3-^{8}FLG" had the sequence AVGIGALFLGFLGAAGSTM-GARSKKKA$_\beta$ and was labeled with ^{13}CO at F8, L9, and G10, and "HFP4", "HFP4-^{6}A", and "HFP4-^{14}A" had the sequence AVGIGALFLGFLGAAGSTMGARSWKKKKK-KA$_\beta$ and were unlabeled and labeled with ^{13}CO at A6 or A14, respectively. The β-alanine resin used for the HFP3 and HFP4 syntheses had a low degree of substitution which helped to increase the yield. All peptides were synthesized using an ABI (Foster City, CA) 431A peptide synthesizer and FMOC chemistry. Peptides were cleaved from the resin for 2−3 h using either a mixture of trifluoroacetic acid (TFA), water, phenol, thioanisole, ethanedithiol, and water in a 33:2:2:2:1 volume ratio or a mixture of TFA, thioanisole, ethanedithiol, and anisole in a 90:5:3:2 volume ratio. TFA was removed from the cleavage filtrate with nitrogen gas, and peptides were precipitated with cold *tert*-butyl methyl ether. Peptides were purified by reversed-phase high-performance liquid chromatography using a semipreparative C_{18} column and a water−acetonitrile gradient containing 0.1% TFA. Mass spectroscopy was used for peptide identification.

NMR Sample Preparation. Samples were made with the ether-linked lipids DTPC and DTPG because these are commercially available lipids which do not contain carbonyl groups. The liquid crystalline to gel phase transition temperatures of DTPC and DTPG are ∼28 °C and are close to the phase transition temperatures (∼23 °C) of the corollary ester-linked lipids 1,2-dimyristoyl-*sn*-glycero-3-phosphocholine and 1,2-dimyristoyl-*sn*-glycero-3-[phospho-*rac*-(1-glycerol)] (*60*). If NMR samples had been made with the more typical ester-linked lipids, there would be large natural abundance lipid ^{13}CO signals which would overlap with the peptide ^{13}CO signals (*35*). For such samples, analysis of the peptide ^{13}CO−lipid ^{31}P distances would then be complicated by the proximity of the lipid ^{13}CO to lipid ^{31}P. All samples contained a 4:1 DTPC:DTPG molar ratio which reflected the approximate ratio of neutral to negatively charged headgroups in membranes of host cells of HIV (*54*, *57*). For each triply ^{13}CO-labeled HFP, a sample was made with a 4:1 DTPC:DTPG ratio (≡"PC:PG") and a sample was made with an 8:2:5 DTPC:DTPG:cholesterol ratio (≡"PC:PG:CHOL"). The latter total lipid:cholesterol molar ratio reflected the ratio observed in membranes of host cells of HIV, and the former PC:PG composition without cholesterol was similar to membrane compositions used in previous structural studies of fusion peptides (*54*, *57*, *61*−*63*). The samples containing singly ^{13}CO-labeled HFP were prepared with PC:PG:CHOL.

Each sample preparation began with dissolution in chloroform of a total of 20 μmol of PC:PG or 30 μmol of PC:PG:CHOL. The chloroform was removed under a stream of nitrogen followed by overnight vacuum pumping. The lipid film was suspended in 2 mL of buffer and homogenized with 10 freeze−thaw cycles. Large unilamellar vesicles were formed by extrusion through a 100 nm diameter polycarbonate filter (Avestin, Ottawa, ON). HFP (0.8 μmol by weight) was dissolved in 2 mL of buffer, and the HFP and vesicle solutions were then gently vortexed together. The mixture was refrigerated overnight and ultracentrifuged at ∼150000*g* for 5 h. The membrane pellet with associated bound HFP was transferred to a 4 mm diameter magic angle spinning (MAS) NMR rotor. The majority of the HFP binds to membranes under these conditions, and the membranes remain bilayers for an HFP:lipid ratio of ∼0.04 (*27*, *56*, *59*, *64*).

A sample was also prepared for calibration of the NMR experiments and contained HFP4 (0.8 μmol) and DPPC-^{13}C (20 μmol). The ^{13}CO signal of this sample was dominated by DPPC-^{13}C.

Solid-State NMR. Experiments were conducted on a 9.4 T solid-state NMR spectrometer (Varian Infinity Plus, Palo Alto, CA) equipped with a triple-resonance MAS probe. The detection channel was tuned to ^{13}C at 100.8 MHz; the decoupling channel was tuned to ^{1}H at 400.8 MHz, and the third channel was tuned to ^{31}P at 162.2 MHz. ^{13}C shifts were externally referenced to the methylene resonance of adamantane at 40.5 ppm; ^{31}P shifts were referenced to 85% H_3PO_4 at 0 ppm, and the ^{13}C and ^{31}P transmitter chemical shifts were 156 and −16 ppm, respectively. The ^{13}C referencing allowed direct comparison with ^{13}C shift databases derived from liquid-state NMR assignments of proteins (*65*, *66*). These databases are appropriate for solid-state NMR data as evidenced by similar ^{13}C shifts observed for the same protein in either aqueous solution or the microcrystalline state (*67*−*69*). Experiments were conducted at −50 °C to enhance the ^{13}C signal and to prevent motional averaging of the ^{13}C−^{31}P dipolar coupling which was the parameter used to assess HFP location in membranes. The ^{13}C shifts and presumably the HFP conformation were comparable at −50 °C and ambient temperature (*70*). At −50 °C, the lipids were likely in the gel phase for the PC:PG samples and in the liquid-ordered phase for the PC:PG:CHOL samples (*60*, *71*). Analyses of slow-spinning spectra yielded a ^{13}CO chemical shift anisotropy range of approximately 90−240 ppm and a ^{31}P chemical shift anisotropy range of approximately −75 to 100 ppm (*72*). The REDOR experiment included in sequence (1) a 50 kHz ^{1}H $\pi/2$ pulse, (2) 1 ms cross polarization with a 52 kHz ^{1}H field and a 58−69 kHz ramped ^{13}C field, (3) a dephasing period with a duration of τ which contained ∼50 kHz ^{13}C π and in some cases ∼60 kHz ^{31}P π pulses with XY-8 phase cycling on each channel, and (4) ^{13}C detection with a four-scan phase cycle (*29*, *35*, *73*−*75*). Two-pulse phase modulation ^{1}H decoupling of ∼100 kHz was applied during the dephasing and detection periods; the recycle delay was 1 s, and the MAS frequency was 8000 ± 2 Hz (*76*).

For each sample and each τ, two spectra were acquired. The dephasing period during the "S_1" acquisition contained a ^{13}C π pulse at the end of each rotor cycle except for the last cycle and a ^{31}P π pulse in the middle of each cycle. The ^{31}P pulses were absent during the "S_0" acquisition. MAS averaged the ^{13}C−^{31}P dipolar coupling to zero over each rotor cycle of the dephasing period of the S_0 acquisition, while incorporation of two π pulses per rotor cycle during the S_1 acquisition resulted in a non-zero average value of the dipolar coupling and concomitant reduction in signals of ^{13}C nuclei close to ^{31}P. Determination of *d* was based on the difference in the ^{13}C signal intensity of the two spectra.

The ^{1}H and ^{13}C rf fields were initially calibrated with adamantane, and the ^{13}C cross polarization field was then adjusted to give the maximum ^{13}CO signal of the sample containing unlabeled HFP4 and DPPC-^{13}C. The ^{31}P π pulse length was set by minimization of the S_1 signal in this sample for a τ of 8 ms, and the ^{1}H TPPM pulse length was set to give the maximum S_0 signal.

REDOR Data Analysis. All spectra were processed with Gaussian line broadening and with baseline correction. For each sample and each value of τ, spectra were integrated over a defined chemical shift range and the integrals of the S_0 and S_1 spectra were denoted as "S_0" and "S_1" and were used to calculate a normalized experimental dephasing parameter via the relation $(\Delta S/S_0)^{exp} = 1 - (S_1/S_0)$. Uncertainties in $(\Delta S/S_0)^{exp}$ were calculated:

$$\sigma^{exp} = \frac{\sqrt{S_0^{\,2}\sigma_{S_1}^{\,2} + S_1^{\,2}\sigma_{S_0}^{\,2}}}{S_0^{\,2}} \quad (1)$$

where σ_{S_0} and σ_{S_1} were the experimental root-mean-square deviations of integrated intensities in regions of the spectra without signal (*77*). Relative to the other labeled HFP samples, the HFP2-^{14}AAG and HFP4-^{14}A samples had significantly larger values of $(\Delta S/S_0)^{exp}$, and data from these samples were used to determine an approximate distance between the ^{31}P atoms and the labeled ^{13}CO groups. The distance determination was done with $(\Delta S/S_0)^{lab}$ calculated to remove the natural abundance (na) contribution from $(\Delta S/S_0)^{exp}$:

$$\left(\frac{\Delta S}{S_0}\right)^{lab} = \left(1 + \frac{S_0^{na}}{S_0^{lab}}\right)\left(\frac{\Delta S}{S_0}\right)^{exp} - \left(\frac{S_0^{na}}{S_0^{lab}}\right)\left(\frac{\Delta S}{S_0}\right)^{na} \quad (2)$$

The values of (S_0^{na}/S_0^{lab}) were 0.084 and 0.32 for the HFP2-^{14}AAG and HFP4-^{14}A samples, respectively. The values of $(\Delta S/S_0)^{na}$ were calculated as the average of $(\Delta S/S_0)^{exp}$ for the HFP2-^{5}GAL, HFP3-^{8}FLG, and HFP2-^{11}FLG samples and for τ values of 2, 8, 16, and 24 ms were 0.000, 0.029, 0.094, and 0.134 for the PC:PG samples and 0.026, 0.028, 0.083, and 0.092 for the PC:PG:CHOL samples, respectively. The σ^{lab} values were calculated with the equation $\sigma^{lab} = (1 + S_0^{na}/S_0^{lab}) \times \sigma^{exp}$, which neglected the contribution from the far-right term in eq 2. Discussion of this approximation and derivation of eq 2 are given in the Supporting Information.

Simulations of the experimental data were based on a single ^{13}CO$-^{31}$P spin pair model:

$$\left(\frac{\Delta S}{S_0}\right)^{sim} = 1 - [J_0(\sqrt{2}\lambda)]^2 + 2\sum_{k=1}^{5}\frac{[J_k(\sqrt{2}\lambda)]^2}{16k^2 - 1} \quad (3)$$

where $\lambda = d\tau$ and J_k is the kth order Bessel function of the first kind (*78*). The samples contained multiple ^{13}CO$-^{31}$P distances and couplings, and these are approximated as a single r and a single d in eq 3 (*29*, *51*, *79*).

For the HFP4/DPPC-^{13}C sample, $\chi^2(d)$ values were calculated for an array of values of d:

$$\chi^2(d) = \sum_{i=1}^{T}\frac{\left\{\left(\frac{\Delta S}{S_0}\right)_i^{exp} - \left[\frac{\Delta S}{S_0}(d)\right]_i^{sim}\right\}^2}{(\sigma_i^{exp})^2} \quad (4)$$

where T is the number of experimental τ values. The best-fit d corresponded to the minimum $\chi^2(d)$.

At larger τ values, $(\Delta S/S_0)^{lab}$ for the HFP2-^{14}AAG and HFP4-^{14}A samples reached plateau values which were significantly smaller than 1 while the $(\Delta S/S_0)^{sim}$ had plateau values of ~1. This inconsistency was resolved using a model of two populations of membrane-associated HFPs. Fraction f represented ^{13}CO groups close to the lipid ^{31}P atoms with a corresponding non-zero d, while fraction $1 - f$ represented ^{13}CO groups far from the lipid ^{31}P atoms with a corresponding d of 0. Fitting was done with an array of values of d and f:

$$\chi^2(d) = \sum_{i=1}^{T}\frac{\left\{\left(\frac{\Delta S}{S_0}\right)_i^{lab} - f\left[\frac{\Delta S}{S_0}(d)\right]_i^{sim}\right\}^2}{(\sigma_i^{lab})^2} \quad (5)$$

The uncertainty of d was calculated with the $\chi^2 = \chi^2_{min} + 1$ criterion (*77*).

RESULTS

Overall Strategy. Our long-term goal is a detailed structure of the membrane location of the HFP in helical and β strand conformations. Prior to the beginning of this study, there was relatively little information about the membrane location of HFP, particularly for the β strand conformation. It was likely that a large number of ^{13}CO sites had ^{13}CO$-^{31}$P distances beyond the REDOR detection limit. In addition, HFP ^{13}C line widths are fairly broad which leads to overlap of ^{13}CO resonances from different residues and the need for specific ^{13}CO labeling. In an effort to reduce the numbers of specifically labeled peptides needed to develop a membrane location model, samples were first made with four peptides, each of which had ^{13}CO labels at three sequential residues between G5 and G16. The G5$-$G16 region was therefore rapidly scanned for ^{13}CO$-^{31}$P proximity. Although the $(\Delta S/S_0)^{exp}$ data for each of the samples had contributions from three distinct ^{13}CO sites, the individual $(\Delta S/S_0)$ value would be appreciably greater than zero only for ^{13}CO$-^{31}$P distances of $\leq$8 Å. The regions of HFP close to ^{31}P would be defined from the REDOR data on the triply labeled samples, and these regions would then provide a basis for choosing sites for singly ^{13}CO-labeled peptides. ^{13}CO$-^{31}$P distances are more straightforwardly derived from $(\Delta S/S_0)$ values of singly labeled HFPs, and REDOR data for two such HFPs are presented to refine the basic HFP membrane location model developed from the triply labeled HFP data.

REDOR Calibration Experiments. As an initial control experiment, ^{13}CO$-^{31}$P REDOR spectra were obtained for HFP2-^{11}FLG lyophilized from water and resulted in a $(\Delta S/S_0)^{exp}$ of ~0 for values of τ between 1 and 19 ms (Figure 1a$-$c). Non-zero values of $(\Delta S/S_0)^{exp}$ for ^{13}CO groups in

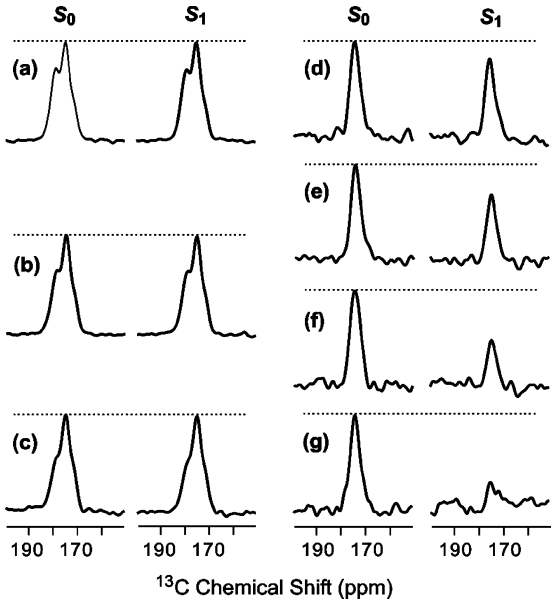

FIGURE 1: ^{13}CO−^{31}P REDOR spectra of (a−c) lyophilized HFP2-^{11}FLG and (d−g) the HFP4/DPPC-^{13}C sample. The left and right spectra in each pair of ^{13}C-detected spectra are S_0 and S_1 spectra, respectively. The dotted lines are drawn for visual comparison of S_0 and S_1 peak intensities. Each spectrum was processed with 200 Hz Gaussian line broadening and baseline correction. The τ values and numbers of S_0 or S_1 scans in each pair of spectra were as follows: (a) 1 ms and 120, (b) 11 ms and 126, (c) 19 ms and 138, (d) 1 ms and 8, (e) 7 ms and 56, (f) 13 ms and 104, and (g) 19 ms and 152, respectively.

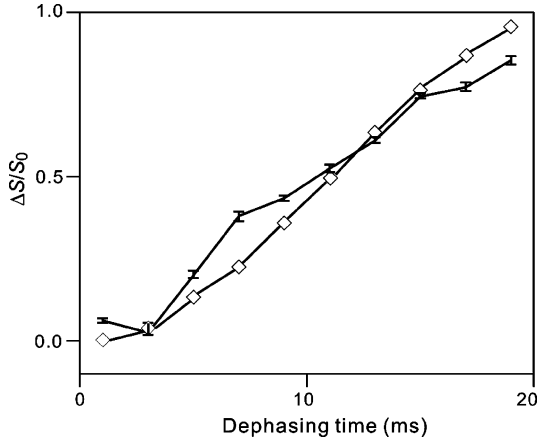

FIGURE 2: $(\Delta S/S_0)^{exp}$ (vertical lines with error bars) and best-fit $(\Delta S/S_0)^{sim}$ (◇) vs dephasing time (τ) for the HFP4/DPPC-1-^{13}C sample. Lines are drawn between points with adjacent values of τ. Each $(\Delta S/S_0)^{exp}$ value was obtained from a 1 ppm integration region centered at 173 ppm. The total $S_0 + S_1$ numbers of scans for τ values of 1, 3, 5, 7, 9, 11, 13, 15, 17, and 19 ms were 16, 48, 80, 112, 144, 176, 208, 240, 272, and 304, respectively. The displayed best-fit $(\Delta S/S_0)^{sim}$ values corresponded to a d of 68 Hz and an r of 5.6 Å.

membrane-associated HFP samples can therefore be definitively ascribed to ^{13}CO−^{31}P proximity. As displayed in Figure 1d−g, REDOR spectra were also obtained for the HFP4/DPPC-^{13}C sample. Because HFP4 is unlabeled and DPPC-^{13}C is labeled, the signals were primarily due to the DPPC ^{13}CO groups and have non-zero $(\Delta S/S_0)^{exp}$ values because of the proximity of the headgroup ^{31}P. Figure 2 displays $(\Delta S/S_0)^{exp}$ and best-fit $(\Delta S/S_0)^{sim}$ for this sample and yielded a d of 68 Hz and an r of 5.6 Å. The best-fit NMR value of r is comparable to the r values of 5−6 Å observed

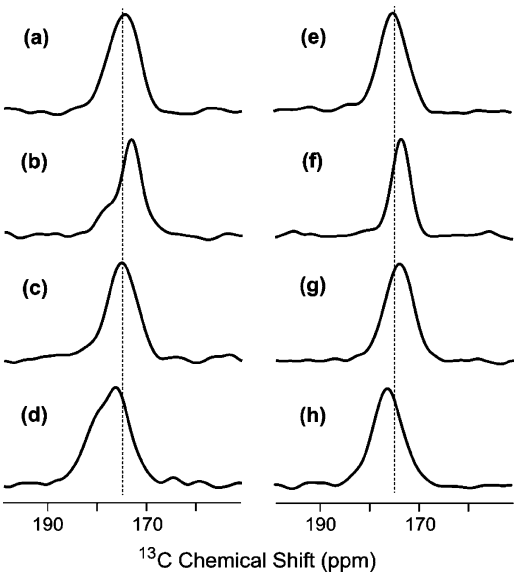

FIGURE 3: S_0 spectra for membrane-associated HFP with a peptide:lipid ratio of ~0.04. The dotted lines are at 175 ppm. All spectra were obtained with a τ of 2 ms and were processed with 200 Hz Gaussian line broadening and baseline correction. The membrane composition for samples a−d was PC:PG, and the membrane composition for samples e−h was PC:PG:CHOL: (a and e) HFP2-^{5}GAL, (b and f) HFP3-^{8}FLG, (c and g) HFP2-^{11}FLG, and (d and h) HFP2-^{14}AAG. The numbers of scans summed to obtain spectra a−h were 4823, 3867, 4823, 8500, 3259, 1001, 4320, and 6992, respectively.

in the crystal structures of the related lipids, 1,2-dimyristoyl-*sn*-glycero-3-phosphocholine and 1,2-dipalmitoyl-*sn*-glycero-[phospho-*rac*-(1-glycerol)] (which had both been dehydrated) and in molecular dynamics simulations of gel-phase DPPC (*80*−*82*). The differences between $(\Delta S/S_0)^{exp}$ and $(\Delta S/S_0)^{sim}$ are likely due to (1) contributions to $(\Delta S/S_0)^{exp}$ from intra- and intermolecular ^{31}P with comparable values of r which contrasts with the single ^{13}CO−^{31}P spin pair model used to calculate $(\Delta S/S_0)^{sim}$, (2) two structurally distinct ^{13}CO groups in each headgroup with different intra- and intermolecular r values, and (3) structural disorder within the headgroups (*79*). Overall, the DPPC-^{13}C fitting yielded good agreement between the NMR r value and the expected range of r values in the lipid.

For the HFP4/DPPC-^{13}C sample, experiments were also conducted with a "one-channel" version of the REDOR sequence for which the S_1 acquisitions contained a single ^{13}C π pulse at the center of the dephasing period and ^{31}P π pulses in the middle and end of each rotor cycle except for the center and end of the dephasing period. The S_0 acquisition did not have ^{31}P π pulses. Relative to the "two-channel" version of REDOR described in Materials and Methods, one-channel REDOR has a reduced number of ^{13}C π pulses which could result in reduced ^{13}C−^{13}C dipolar coupling and larger overall signals (*83*, *84*). In fact, the experimental S_0 intensities were comparable for the two versions of REDOR, while $(\Delta S/S_0)^{exp}$ for one-channel REDOR was ~$^{2}/_{3}$ of that of two-channel REDOR (*29*). All subsequent experiments were conducted with two-channel REDOR.

Triply Labeled HFP. The local peptide conformation was examined by analysis of the ^{13}CO chemical shift distributions in S_0 spectra of HFPs obtained with a τ of 2 ms (cf. Figure 3). The data supported the following models. (1) The major fraction of peptides in PC:PG and PC:PG:CHOL

adopted a β strand conformation from G5 to G16, and (2) there is a minor fraction of peptides in PC:PG with helical conformation. The detailed experimental support for the models is based on the known correlation between larger ^{13}CO chemical shifts and local helical conformation and smaller ^{13}CO chemical shifts and local β strand conformation. For example, average database values in parts per million of ^{13}CO chemical shifts of helix (strand) conformations are 175.5 (172.6) for Gly, 179.4 (176.1) for Ala, 178.5 (175.7) for Leu, and 177.1 (174.2) for Phe (*66*). For the HFP2-^{5}GAL, HFP3-^{8}FLG, HFP2-^{11}FLG, and HFP2-^{14}AAG samples, the peak chemical shifts were ~175, 174, 175, and 176 ppm, respectively, and correlated with β strand conformation for the Ala, Leu, and Phe residues. For the HFP3-^{8}FLG and HFP2-^{14}AAG samples associated with PC:PG, there were shoulders at ~178 and 179 ppm, respectively, which correlated with the helical conformation of Ala, Leu, and Phe residues. These results were consistent with previous studies of the conformation of membrane-associated HFP with a peptide:lipid ratio of ~0.04 and with previous observations of a stronger preference for β strand conformation in cholesterol-containing membranes (*27*, *28*, *35*, *55*, *56*, *59*, *70*).

Figure 4 displays the $\tau = 16$ and 24 ms REDOR spectra of triply labeled membrane-associated HFP samples, and Figure 5a,b displays comparative plots of $(\Delta S/S_0)^{exp}$ for the different samples. The data demonstrated that samples containing HFP2-^{14}AAG have qualitatively larger $(\Delta S/S_0)^{exp}$ values than do samples containing HFP labeled at other residues. Using the conformational results from Figure 3, it appears (1) a significant fraction of β strand HFP is in close contact with membranes and (2) the ^{14}AAG (A14−G16) region is closer to the lipid ^{31}P than is the ^{5}GALFLGFLG (G5−G13) region. Figure 5c,d displays plots of $(\Delta S/S_0)^{lab}$ and best-fit $(\Delta S/S_0)^{sim}$ for HFP2-^{14}AAG in PC:PG and PC:PG:CHOL. The best-fit r was ~5.2 Å in both membrane compositions, and the best-fit f values in PC:PG and PC:PG:CHOL were 0.45 and 0.32, respectively. It was not possible to fit the HFP2-^{14}AAG data well without inclusion of the f parameter. Although $(\Delta S/S_0)^{lab}$ had contributions from three ^{13}CO sites which would each have a distinct r, the number of data points and signal-to-noise dictated fitting to a single r value. The best-fit r should therefore be considered as both approximate and as likely representing the population of ^{13}CO sites with the greatest d and smallest r. Fitting was not done for data from the other samples because of the small $(\Delta S/S_0)^{exp}$ and because the $(\Delta S/S_0)^{exp}$ values do not always reach asymptotic values at large τ.

Spectra were also obtained for samples made with HFP1-^{8}FLG, the peptide which did not contain C-terminal lysines. When $\tau = 2$, 8, 16, and 24 ms, $(\Delta S/S_0)^{exp} = -0.02$, 0.06, 0.11, and 0.08 for the HFP1-^{8}FLG/PC:PG sample and 0.01, 0.03, 0.01, and −0.01 for the HFP1-^{8}FLG/PC:PG:CHOL sample, respectively. These values correlated with the $(\Delta S/S_0)^{exp}$ of the respective HFP3-^{8}FLG/PC:PG and HFP3-^{8}FLG/PC:PG:CHOL samples (circles in Figure 5) and suggested that the additional C-terminal lysines of HFP2 and HFP3 do not greatly affect the REDOR results.

Singly Labeled HFP. The triply labeled HFP results motivated experiments on singly labeled HFP4-^{6}A and HFP4-^{14}A associated with PC:PG:CHOL. As discussed in Overall Strategy, analysis of singly labeled HFP data should result in more quantitative assessment of r. In addition, we were interested in studying HFP in a single conformation, and the Figure 3 data suggested that this was best achieved with PC:PG:CHOL and the resulting predominant β strand conformation. Finally, the Figure 5 data suggested that $(\Delta S/S_0)^{lab}$ would be ~0 for a HFP4-^{6}A/PC:PG:CHOL sample and could be non-zero for a HFP4-^{14}A/PC:PG:CHOL sample. REDOR data from these two sites could therefore further test the qualitative membrane location model derived from the triply labeled HFP results.

Figure 6a,b displays the respective S_0 spectra at $\tau = 8$ ms for HFP4-^{6}A and HFP4-^{14}A associated with PC:PG:CHOL.

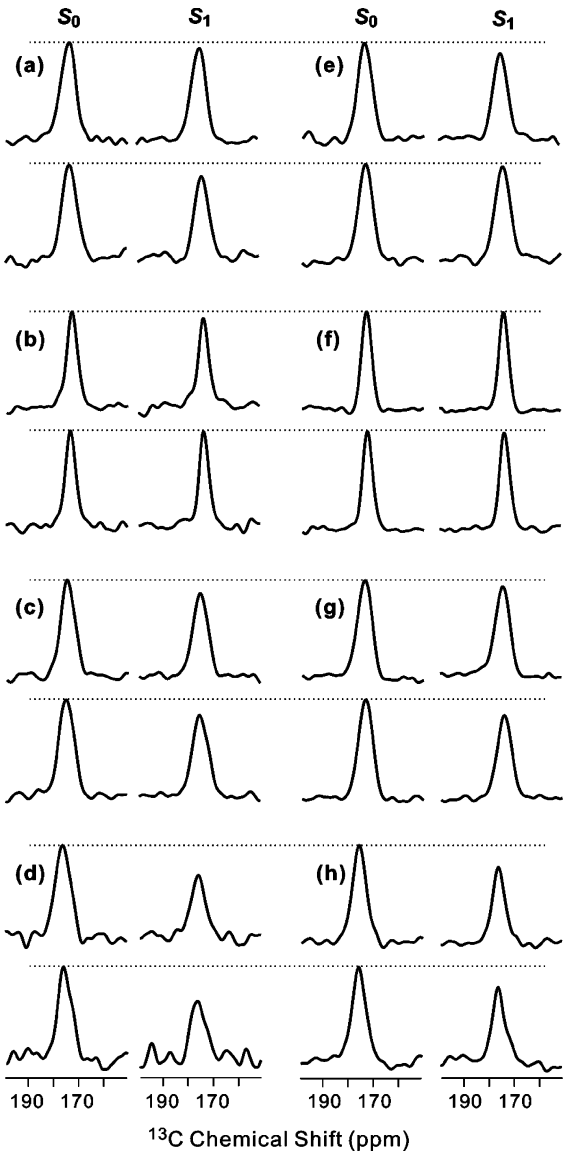

FIGURE 4: ^{13}CO−^{31}P REDOR spectra of membrane-associated HFP with a peptide:lipid ratio of ~0.04. Each letter corresponds to a single sample which contained (a−d) PC:PG or (e−h) PC:PG:CHOL and (a and e) HFP2-^{5}GAL, (b and f) HFP3-^{8}FLG, (c and g) HFP2-^{11}FLG, or (d and h) HFP2-^{14}AAG. For each sample, S_0 (left), S_1 (right), $\tau = 16$ ms (top), and $\tau = 24$ ms (bottom) spectra are displayed. The dotted lines are drawn for visual comparison of S_0 and S_1 peak intensities. Each spectrum was processed with 300 Hz Gaussian line broadening and baseline correction. The numbers of S_0 or S_1 scans summed to obtain the top and bottom spectra were as follows: (a) 30 000 and 56 000, (b) 27 509 and 29 463, (c) 20 000 and 40 000, (d) 44 129 and 48 296, (e) 8448 and 52 384, (f) 5488 and 21 664, (g) 28 032 and 52 384, and (h) 22 576 and 50 240, respectively.

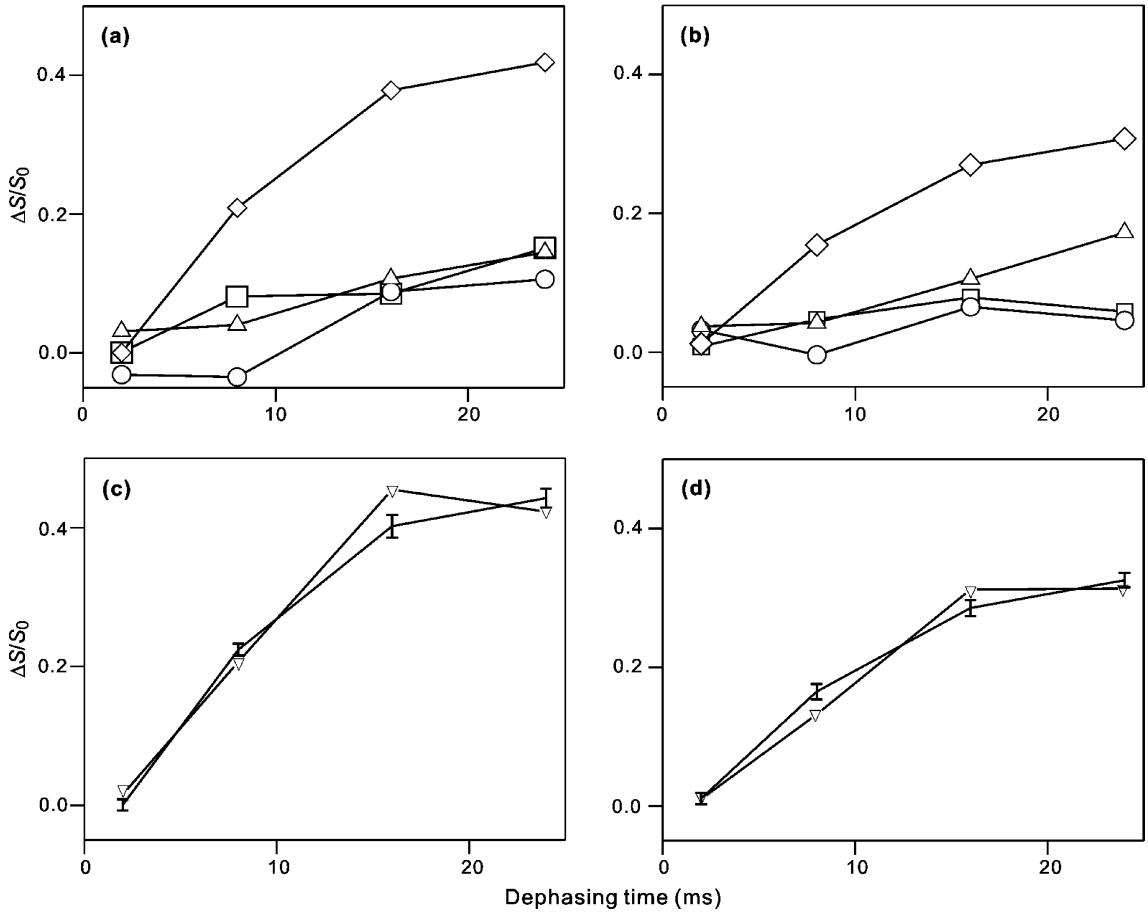

FIGURE 5: $\Delta S/S_0$ vs dephasing time for membrane-associated HFP in (a and c) PC:PG or (b and d) PC:PG:CHOL. For panels a and b, the points correspond to $(\Delta S/S_0)^{exp}$: (□) HFP2-^{5}GAL, (○) HFP3-^{8}FLG, (△) HFP2-^{11}FLG, and (◇) HFP2-^{14}AAG. The vertical dimensions of each symbol approximately correspond to the $\pm 1\sigma$ uncertainty limits. Lines are drawn between $(\Delta S/S_0)^{exp}$ values with adjacent values of τ. Each $(\Delta S/S_0)^{exp}$ value was determined by integration of 10 ppm regions of the S_0 and S_1 spectra. Panels c and d correspond to the HFP2-^{14}AAG/PC:PG and the HFP2-^{14}AAG/PC:PG:CHOL samples, respectively, and the points correspond to $(\Delta S/S_0)^{lab}$ (vertical lines with error bars) and best-fit $(\Delta S/S_0)^{sim}$ (▽). Lines are drawn between points with adjacent τ values. For plot c, the best-fit $d = 91 \pm 8$ Hz with $r = 5.12 \pm 0.16$ Å, $f = 0.45 \pm 0.02$, and $\chi_{min}^2 = 5.0$. For plot d, the best-fit $d = 85 \pm 6$ Hz with $r = 5.24 \pm 0.13$ Å, $f = 0.32 \pm 0.02$, and $\chi_{min}^2 = 3.8$.

Single peaks were observed with peak shifts of ∼175 ppm which correlated with β strand conformation at these residues. The spectrum of HFP4-^{14}A is similar to a difference spectrum representing the Ala-14 ^{13}CO signal for HFP (with no lysines) associated with an ester-linked lipid and cholesterol composition close to that of host cells of HIV (*27*). Figure 6c,d displays the $\tau = 16$ and 24 ms REDOR spectra of the singly labeled HFP4 samples, and Figure 7 shows $(\Delta S/S_0)^{exp}$ plots and data fitting for the HFP4-^{14}A data. At large τ values, $(\Delta S/S_0)^{exp} \approx 0$ for the HFP4-^{6}A sample and $(\Delta S/S_0)^{exp}$ values were significantly greater than zero for the HFP4-^{14}A sample. Fitting of the HFP4-^{14}A data with a single ^{13}CO−^{31}P spin pair model yielded best-fit r and f values of 5.1 Å and 0.29, respectively. Thus, there was general consistency between the REDOR data of the HFP4-^{6}A/PC:PG:CHOL and HFP2-^{5}GAL/PC:PG:CHOL samples and the REDOR data and fitting of the HFP4-^{14}A/PC:PG:CHOL and HFP2-^{14}AAG/PC:PG:CHOL samples.

DISCUSSION

Insertion Models. The position of the HFP in the membrane has been postulated to be a significant structural factor in its fusion activity, and to our knowledge, this study is the first example of direct distance measurements between the HFP and the lipid headgroups. Values of r of ∼5−6 Å were detected between the ^{13}CO groups of residues from A14 to G16 and the lipid ^{31}P atoms. These r values support intimate association of the HFP and membranes containing either only phospholipids or phospholipids and cholesterol. The average r for ^{5}GALFLGFLG ^{13}CO groups was likely greater than 8 Å ($d \leq 25$ Hz) as evidenced by the significantly smaller $(\Delta S/S_0)^{exp}$ (cf. Figures 5 and 7). Thus, relative to the ^{5}GALFLGFLG residues, the ^{14}AAG residues are much closer to the lipid ^{31}P.

The G5−G16 ^{13}CO chemical shift distributions of this study were consistent with a major population of HFP with β strand conformation for these residues. This result correlated with previous studies which supported the following structural features. (1) β strand HFP was fully extended between A1 and G16. (2) β strand HFP formed hydrogen-bonded oligomers or aggregates. (3) A significant fraction of the oligomers have an antiparallel arrangement with adjacent strand crossing between F8 and L9 (*25*, *27*−*29*, *35*, *37*, *85*, *86*). Some of these studies also supported conformational disorder at A21 (*27*, *28*). Although there are some data supporting a population of parallel strand arrangement, "partial membrane insertion (PMI)" and "full membrane insertion (FMI)" models are only presented for the antipar-

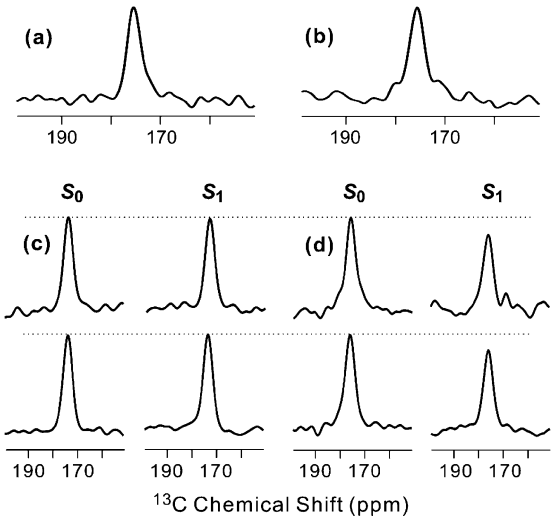

FIGURE 6: ^{13}CO−^{31}P REDOR spectra of (a and c) HFP4-^{6}A/PC:PG:CHOL and (b and d) HFP4-^{14}A/PC:PG:CHOL samples with a peptide:lipid ratio of ~0.04. Panels a and b show S_0 spectra obtained with a τ of 8 ms and processed with 200 Hz Guassian line broadening and baseline correction. Panels c and d show S_0 (left), S_1 (right), $\tau = 16$ ms (top), and $\tau = 24$ ms (bottom) spectra. The dotted lines are drawn for visual comparison of S_0 and S_1 peak intensities. Each spectrum was processed with 300 Hz Gaussian line broadening and baseline correction. The numbers of S_0 or S_1 scans summed were (a) 2304, (b) 3680, (c) 5504 (top) and 28 288 (bottom), and (d) 5120 (top) and 28 736 (bottom).

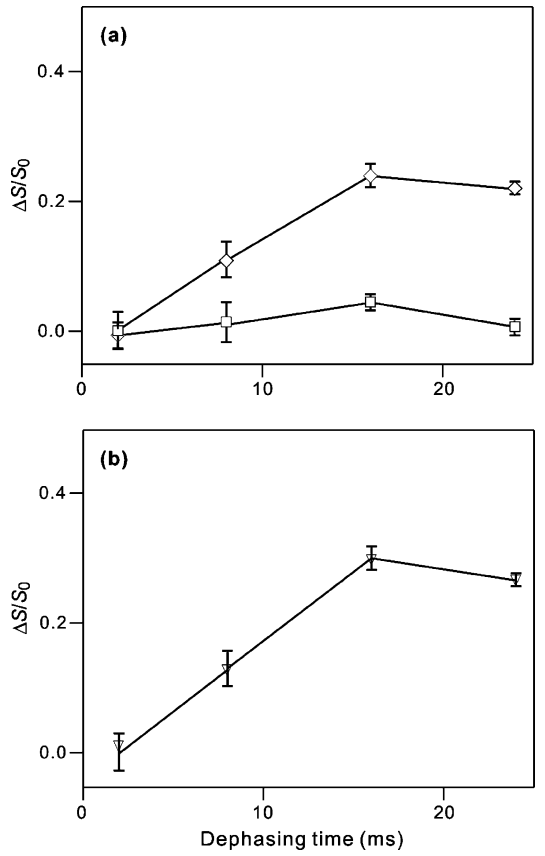

FIGURE 7: $\Delta S/S_0$ vs dephasing time for HFP4-^{6}A/PC:PG:CHOL and HFP-^{14}A/PC:PG:CHOL samples. In panel a, $(\Delta S/S_0)^{exp}$ points with error bars are displayed: HFP4-^{6}A (□) and HFP4-^{14}A (◇). Each $(\Delta S/S_0)^{exp}$ value was determined from integrals of the entire S_0 and S_1 peaks. Panel b represents analysis of the HFP4-^{14}A data: $(\Delta S/S_0)^{lab}$ (vertical lines with error bars) and best-fit $(\Delta S/S_0)^{sim}$ (▽). Lines are drawn between points with adjacent τ values. The best-fit parameters were as follows: $d = 93 \pm 10$ Hz with $r = 5.08 \pm 0.19$ Å, $f = 0.29 \pm 0.02$, and $\chi_{min}^2 = 0.1$.

allel arrangement (cf. Figure 8) (*29*, *35*, *87*). There have been high-resolution structures for the ~130-residue "soluble ectodomain" region of gp41 which begins ~10 residues C-terminal of the HFP and ends ~20 residues N-terminal of the gp41 transmembrane domain (*88*−*92*). These structures showed trimeric gp41 with the residues closest to the HFPs in a parallel in-register coiled coil. Antiparallel HFP strand arrangement in the context of gp41 would then require at least two gp41 trimers. Strands from trimer A (A_1, A_2, and A_3) would be parallel to one another; strands from trimer B (B_1, B_2, and B_3) would be parallel to one another, and an antiparallel interleaved strand arrangement could be formed ($A_1B_3A_2B_2A_3B_1$). There is solid-state NMR evidence for the antiparallel arrangement of membrane-associated HFPs which were cross-linked at their C-termini (*35*).

For antiparallel strands between A1 and G16, the ^{14}AAG residues in both the PMI and FMI models are at the ends of the hydrogen-bonded oligomer and are closer to the lipid headgroups than residues ^{5}GALFLGFLG. The F8 and L9 residues are at the center of the hydrogen-bonded oligomer and are most deeply membrane-inserted in all models. This result is consistent with the smallest $(\Delta S/S_0)^{exp}$ values observed for the HFP1-^{8}FLG and HFP3-^{8}FLG samples and with the large number of apolar side chains in the central ^{7}LFLGFL (L7−L12) region. Relative to the HFP1-^{8}FLG and HFP3-^{8}FLG samples, the models also predict smaller r and larger $(\Delta S/S_0)^{exp}$ values for the HFP2-^{5}GAL and HFP2-^{11}-FLG samples which generally correlate with the experimental data (cf. Figure 5a,b). The models suggest small r and significant $(\Delta S/S_0)^{exp}$ values for HFPs labeled at the N-terminal residues, and future studies could examine samples labeled in this manner.

The PMI model in Figure 8a would likely perturb the membrane and has some similarity with (1) the PMI of extended conformation internal fusion peptides postulated from structures of dengue, Semliki forest, herpes, and vesicular stomatitis viral fusion proteins, (2) the PMI of helical influenza fusion peptide determined from electron spin resonance experiments, and (3) a PMI model based on the HFP-F8W fluorescence measurements (*37*, *61*, *62*, *93*−*96*). However, the locations of lipids in the perturbed leaflet in the PMI model are not clear. For the FMI model of Figure 8b, the positions of the lipids are more clear, but there are non-hydrogen-bonded CO and NH groups at the sheet edges with large Born energies. These energies would be reduced for a FMI β barrel structure (Figure 8c). There is a correlation between the FMI model and the deep insertion of the Trp side chain suggested from fluorescence studies of the HFP-F8W mutant (*36*, *37*). In the context of gp41, individual HFP trimers would be on the same side of the membrane in the PMI model but would be on different sides of the membrane in the FMI model. It is not clear how this FMI trimer topology would relate to the positions of the viral membrane-anchored gp41 trimers and the host cell membranes. The free energy difference between the A1−G16 FMI state and a noninserted state is ~3.9 kJ/mol, as calculated from the sum of individual residue free energy values derived from transmembrane helices (*97*). The calculated difference for the I4−G13 sequence is −2.3 kJ/mol and leads to the general conclusion that the free energy calculations do not strongly distinguish between the PMI and FMI models.

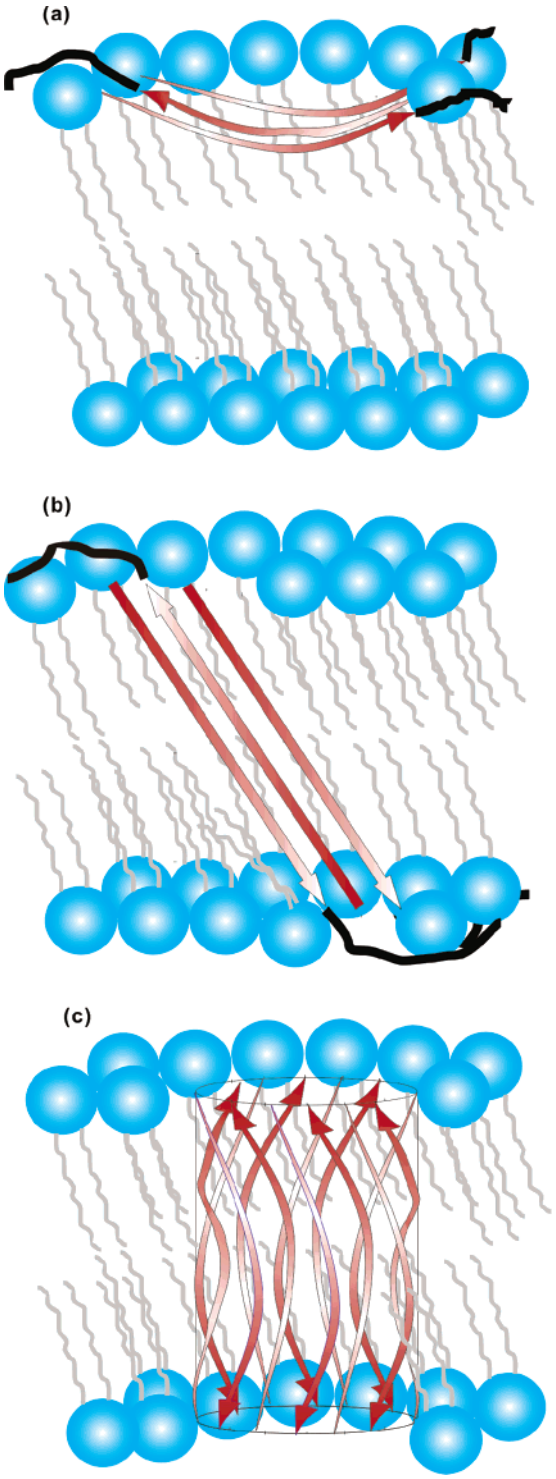

FIGURE 8: (a) Partial membrane insertion (PMI) and (b and c) full membrane insertion (FMI) models for antiparallel β strand HFP. The red arrows represent the A1−G16 residues in the strand conformation, and the black lines represent the S17−S23 residues in random coil conformations. For clarity, black lines are not displayed in panel c. Lipids are colored blue and gray, and cholesterol is not displayed. Three antiparallel strands are displayed in panels a and b and 12 strands in panel c, but the actual number of strands in the oligomer or aggregate is not known. The curvature and angle of the strands with respect to the bilayer normal are not known, but the models consider that A1−G16 is ~55 Å long and that the transbilayer distance is ~48 Å (*100*). The experiments do not provide information about the membrane locations of residues S17−S23. Relative to the FMI model (b), the FMI β barrel variant (c) could have reduced energy because all of the residues in the membrane interior have backbone hydrogen bonds.

Future studies could discriminate between the PMI and FMI models using REDOR distance measurements between peptide nuclei and lipid acyl chain nuclei (*51*).

There are similarities between these PMI and FMI models of oligomeric β strand HFP and PMI and FMI models which have been developed for a single HFP in a helical conformation (*38*, *39*, *98*). Much of the experimental data for helical HFP insertion has been based on detergent rather than membrane samples, and there has been support for both micelle surface location and micelle traversal by HFP (*19*−*23*). Our results on oligomeric β strand HFP were consistent with the previous observations that the A15 and G16 residues of monomeric helical HFP were close to the water−micelle interface and that the F8−G10 residues were farthest from this interface. Thus, there may be common features shared by the micelle and membrane locations of helical and β strand HFP.

Origin of f and Effects of Cholesterol. The HFP2-^{14}AAG and HFP4-^{14}A data could only be fit well with addition of the *f* parameter which approximately reflected the fractional population of peptides whose labeled residues were close to the ^{31}P. Analysis of ^{13}CO−^{31}P REDOR data of a membrane-associated antimicrobial peptide also required an *f* parameter, and the best-fit *f* and *r* values were similar to our results (*51*).

The membranes of host cells of HIV have a cholesterol:lipid ratio of ~0.45, and the membranes of HIV have a cholesterol:lipid ratio of ~0.8 (*54*, *57*). These data suggest that it is interesting to probe the effect of cholesterol on HFP location in the membrane. Similar values of $(\Delta S/S_0)^{exp}$ were obtained for the ^{5}GALFLGFLG residues in PC:PG and PC:PG:CHOL samples, and the best-fit *r* values for the ^{14}AAG residues were comparable in both membrane compositions. These results suggest (1) the inserted HFP population has a similar location in membranes with or without cholesterol and (2) the membrane location of the A14−G16 residues may be similar in both helical and β strand conformations because there appeared to be some helical conformation in PC:PG and negligible helical conformation in PC:PG:CHOL. There was a difference in the best-fit *f* for HFP2-^{14}AAG in PC:PG and PC:PG:CHOL with values of 0.45 and 0.32, respectively. There are several potential explanations for this variation. First, the HFP/PC:PG samples likely had a small population of helical conformation which was absent in the HFP/PC:PG:CHOL samples, and this helical population could have contributed to the larger *f* in PC:PG. Second, the presumably gel phase PC:PG and the liquid-ordered phase PC:PG:CHOL had lateral molecular densities of ~0.213 and ~0.256 Å^{-2}, respectively, as calculated from gel-phase PC and PG areas of 47 Å^2, liquid-ordered PC and PG areas of 40 Å^2, and a cholesterol area of 37 Å^2 (*60*, *71*, *99*, *100*). The denser packing in PC:PG:CHOL could have shifted an inserted HFP−surface HFP equilibrium to surface HFP and led to a reduced *f*. Finally, relative to the PC:PG sample, there was likely a reduced number of phospholipids close to the ^{14}AAG residues in the PC:PG:CHOL sample because of statistical substitution of nearby phospholipids with cholesterol. This lipid dilution may have also reduced *f* in the PC:PG:CHOL sample.

In summary, ^{13}CO−^{31}P distance measurements have demonstrated the proximity of the ^{14}AAG residues to the lipid ^{31}P for a significant fraction of membrane-associated

HFP. This proximity was observed for both membranes with and without cholesterol. The chemical shifts of this study as well as results from previous studies correlated with a predominant population of HFP with β strand conformation. Models of partial and full insertion of β strands are proposed which are consistent with the experimental data. Although there have been numerous previous observations of β strand HFP, the role of this conformation in fusion has been controversial (*14*, *16*, *18*, *31*, *45*). This study demonstrates that β strand HFP is in intimate contact with membranes and merits serious consideration as a fusogenic conformation.

Interesting future work could include studies of cross-linked HFPs which are thought to mimic the HFP oligomeric topology in the gp41 protein and which have increased fusion rates relative to the non-cross-linked HFPs of this study (*34*). There may be a distinct membrane location of the cross-linked HFPs which correlates with their fast fusion rate. It is also known that the cross-linked HFP trimer will form helical or β strand conformation in membranes without or with cholesterol, respectively, so that studies of the trimer in different membrane compositions can provide information about the conformational dependence of peptide location in membranes (*35*).

ACKNOWLEDGMENT

Dr. Richard Venable provided the coordinates of crystalline DMPC and gel-phase DPPC. We acknowledge Dr. Michael Feig for useful discussions about the insertion models.

SUPPORTING INFORMATION AVAILABLE

Equation 2 and the σ^{lab} expression are derived and discussed. This material is available free of charge via the Internet at http://pubs.acs.org.

REFERENCES

1. Hernandez, L. D., Hoffman, L. R., Wolfsberg, T. G., and White, J. M. (1996) Virus-cell and cell-cell fusion, *Annu. Rev. Cell Dev. Biol. 12*, 627−661.
2. Eckert, D. M., and Kim, P. S. (2001) Mechanisms of viral membrane fusion and its inhibition, *Annu. Rev. Biochem. 70*, 777−810.
3. Jahn, R., Lang, T., and Sudhof, T. C. (2003) Membrane fusion, *Cell 112*, 519−533.
4. Blumenthal, R., Clague, M. J., Durell, S. R., and Epand, R. M. (2003) Membrane fusion, *Chem. Rev. 103*, 53−69.
5. Bentz, J. (2000) Membrane fusion mediated by coiled coils: A hypothesis, *Biophys. J. 78*, 886−900.
6. Chernomordik, L. V., and Kozlov, M. M. (2003) Protein-lipid interplay in fusion and fission of biological membranes, *Annu. Rev. Biochem. 72*, 175−207.
7. Cohen, F. S., and Melikyan, G. B. (2004) The energetics of membrane fusion from binding, through hemifusion, pore formation, and pore enlargement, *J. Membr. Biol. 199*, 1−14.
8. Turner, B. G., and Summers, M. F. (1999) Structural biology of HIV, *J. Mol. Biol. 285*, 1−32.
9. Colman, P. M., and Lawrence, M. C. (2003) The structural biology of type I viral membrane fusion, *Nat. Rev. Mol. Cell Biol. 4*, 309−319.
10. Freed, E. O., Myers, D. J., and Risser, R. (1990) Characterization of the fusion domain of the human immunodeficiency virus type 1 envelope glycoprotein gp41, *Proc. Natl. Acad. Sci. U.S.A. 87*, 4650−4654.
11. Freed, E. O., Delwart, E. L., Buchschacher, G. L., Jr., and Panganiban, A. T. (1992) A mutation in the human immunodeficiency virus type 1 transmembrane glycoprotein gp41 dominantly interferes with fusion and infectivity, *Proc. Natl. Acad. Sci. U.S.A. 89*, 70−74.
12. Schaal, H., Klein, M., Gehrmann, P., Adams, O., and Scheid, A. (1995) Requirement of N-terminal amino acid residues of gp41 for human immunodeficiency virus type 1-mediated cell fusion, *J. Virol. 69*, 3308−3314.
13. Delahunty, M. D., Rhee, I., Freed, E. O., and Bonifacino, J. S. (1996) Mutational analysis of the fusion peptide of the human immunodeficiency virus type 1: Identification of critical glycine residues, *Virology 218*, 94−102.
14. Durell, S. R., Martin, I., Ruysschaert, J. M., Shai, Y., and Blumenthal, R. (1997) What studies of fusion peptides tell us about viral envelope glycoprotein-mediated membrane fusion, *Mol. Membr. Biol. 14*, 97−112.
15. Kliger, Y., Aharoni, A., Rapaport, D., Jones, P., Blumenthal, R., and Shai, Y. (1997) Fusion peptides derived from the HIV type 1 glycoprotein 41 associate within phospholipid membranes and inhibit cell-cell fusion. Structure-function study, *J. Biol. Chem. 272*, 13496−13505.
16. Pereira, F. B., Goni, F. M., Muga, A., and Nieva, J. L. (1997) Permeabilization and fusion of uncharged lipid vesicles induced by the HIV-1 fusion peptide adopting an extended conformation: Dose and sequence effects, *Biophys. J. 73*, 1977−1986.
17. Pritsker, M., Rucker, J., Hoffman, T. L., Doms, R. W., and Shai, Y. (1999) Effect of nonpolar substitutions of the conserved Phe11 in the fusion peptide of HIV-1 gp41 on its function, structure, and organization in membranes, *Biochemistry 38*, 11359−11371.
18. Martin, I., Schaal, H., Scheid, A., and Ruysschaert, J. M. (1996) Lipid membrane fusion induced by the human immunodeficiency virus type 1 gp41 N-terminal extremity is determined by its orientation in the lipid bilayer, *J. Virol. 70*, 298−304.
19. Chang, D. K., Cheng, S. F., and Chien, W. J. (1997) The amino-terminal fusion domain peptide of human immunodeficiency virus type 1 gp41 inserts into the sodium dodecyl sulfate micelle primarily as a helix with a conserved glycine at the micelle-water interface, *J. Virol. 71*, 6593−6602.
20. Jaroniec, C. P., Kaufman, J. D., Stahl, S. J., Viard, M., Blumenthal, R., Wingfield, P. T., and Bax, A. (2005) Structure and dynamics of micelle-associated human immunodeficiency virus gp41 fusion domain, *Biochemistry 44*, 16167−16180.
21. Morris, K. F., Gao, X. F., and Wong, T. C. (2004) The interactions of the HIV gp41 fusion peptides with zwitterionic membrane mimics determined by NMR spectroscopy, *Biochim. Biophys. Acta 1667*, 67−81.
22. Chang, D. K., and Cheng, S. F. (1998) Determination of the equilibrium micelle-inserting position of the fusion peptide of gp41 of human immunodeficiency virus type 1 at amino acid resolution by exchange broadening of amide proton resonances, *J. Biomol. NMR 12*, 549−552.
23. Langham, A., and Kaznessis, Y. (2005) Simulation of the N-terminus of HIV-1 glycoprotein 41000 fusion peptide in micelles, *J. Pept. Sci. 11*, 215−224.
24. Rafalski, M., Lear, J. D., and DeGrado, W. F. (1990) Phospholipid interactions of synthetic peptides representing the N-terminus of HIV gp41, *Biochemistry 29*, 7917−7922.
25. Nieva, J. L., Nir, S., Muga, A., Goni, F. M., and Wilschut, J. (1994) Interaction of the HIV-1 fusion peptide with phospholipid vesicles: Different structural requirements for fusion and leakage, *Biochemistry 33*, 3201−3209.
26. Peisajovich, S. G., Epand, R. F., Pritsker, M., Shai, Y., and Epand, R. M. (2000) The polar region consecutive to the HIV fusion peptide participates in membrane fusion, *Biochemistry 39*, 1826−1833.
27. Yang, J., Gabrys, C. M., and Weliky, D. P. (2001) Solid-state nuclear magnetic resonance evidence for an extended β strand conformation of the membrane-bound HIV-1 fusion peptide, *Biochemistry 40*, 8126−8137.
28. Bodner, M. L. (2006) Solid state nuclear magnetic resonance of the HIV-1 and influenza fusion peptides associated with membranes, Ph.D. Thesis, Michigan State University, East Lansing, MI.
29. Yang, J., and Weliky, D. P. (2003) Solid state nuclear magnetic resonance evidence for parallel and antiparallel strand arrangements in the membrane-associated HIV-1 fusion peptide, *Biochemistry 42*, 11879−11890.
30. Gordon, L. M., Curtain, C. C., Zhong, Y. C., Kirkpatrick, A., Mobley, P. W., and Waring, A. J. (1992) The amino-terminal peptide of HIV-1 glycoprotein 41 interacts with human erythrocyte

membranes: Peptide conformation, orientation and aggregation, *Biochim. Biophys. Acta 1139*, 257−274.
31. Epand, R. M. (2003) Fusion peptides and the mechanism of viral fusion, *Biochim. Biophys. Acta 1614*, 116−121.
32. Afonin, S., Glaser, R. W., Berditchevskaia, M., Wadhwani, P., Guhrs, K. H., Mollmann, U., Perner, A., and Ulrich, A. S. (2003) 4-Fluorophenylglycine as a label for ^{19}F NMR structure analysis of membrane-associated peptides, *ChemBioChem 4*, 1151−1163.
33. Hofmann, M. W., Weise, K., Ollesch, J., Agrawal, P., Stalz, H., Stelzer, W., Hulsbergen, F., de Groot, H., Gerwert, K., Reed, J., and Langosch, D. (2004) De novo design of conformationally flexible transmembrane peptides driving membrane fusion, *Proc. Natl. Acad. Sci. U.S.A. 101*, 14776−14781.
34. Yang, R., Prorok, M., Castellino, F. J., and Weliky, D. P. (2004) A trimeric HIV-1 fusion peptide construct which does not self-associate in aqueous solution and which has 15-fold higher membrane fusion rate, *J. Am. Chem. Soc. 126*, 14722−14723.
35. Zheng, Z., Yang, R., Bodner, M. L., and Weliky, D. P. (2006) Conformational flexibility and strand arrantements of the membrane-associated HIV fusion peptide trimer probed by solid-state NMR spectroscopy, *Biochemistry 45*, 12960−12975.
36. Agirre, A., Flach, C., Goni, F. M., Mendelsohn, R., Valpuesta, J. M., Wu, F. J., and Nieva, J. L. (2000) Interactions of the HIV-1 fusion peptide with large unilamellar vesicles and monolayers. A cryo-TEM and spectroscopic study, *Biochim. Biophys. Acta 1467*, 153−164.
37. Haque, M. E., Koppaka, V., Axelsen, P. H., and Lentz, B. R. (2005) Properties and structures of the influenza and HIV fusion peptides on lipid membranes: Implications for a role in fusion, *Biophys. J. 89*, 3183−3194.
38. Kamath, S., and Wong, T. C. (2002) Membrane structure of the human immunodeficiency virus gp41 fusion domain by molecular dynamics simulation, *Biophys. J. 83*, 135−143.
39. Maddox, M. W., and Longo, M. L. (2002) Conformational partitioning of the fusion peptide of HIV-1 gp41 and its structural analogs in bilayer membranes, *Biophys. J. 83*, 3088−3096.
40. Grobner, G., Glaubitz, C., and Watts, A. (1999) Probing membrane surfaces and the location of membrane-embedded peptides by ^{13}C MAS NMR using lanthanide ions, *J. Magn. Reson. 141*, 335−339.
41. Buffy, J. J., Hong, T., Yamaguchi, S., Waring, A. J., Lehrer, R. I., and Hong, M. (2003) Solid-state NMR investigation of the depth of insertion of protegrin-1 in lipid bilayers using paramagnetic Mn^{2+}, *Biophys. J. 85*, 2363−2373.
42. Vogel, A., Scheidt, H. A., and Huster, D. (2003) The distribution of lipid attached spin probes in bilayers: Application to membrane protein topology, *Biophys. J. 85*, 1691−1701.
43. Tian, C. L., Gao, P. F., Pinto, L. H., Lamb, R. A., and Cross, T. A. (2003) Initial structural and dynamic characterization of the M2 protein transmembrane and amphipathic helices in lipid bilayers, *Protein Sci. 12*, 2597−2605.
44. Gallagher, G. J., Hong, M., and Thompson, L. K. (2004) Solid-state NMR spin diffusion for measurement of membrane-bound peptide structure: Gramicidin A, *Biochemistry 43*, 7899−7906.
45. Grage, S. L., Afonin, S., Grune, M., and Ulrich, A. S. (2004) Interaction of the fusogenic peptide B18 in its amyloid-state with lipid membranes studied by solid state NMR, *Chem. Phys. Lipids 132*, 65−77.
46. Henzler-Wildman, K. A., Martinez, G. V., Brown, M. F., and Ramamoorthy, A. (2004) Perturbation of the hydrophobic core of lipid bilayers by the human antimicrobial peptide LL-37, *Biochemistry 43*, 8459−8469.
47. Abu-Baker, S., Qi, X. Y., Newstadt, J., and Lorigan, G. A. (2005) Structural changes in a binary mixed phospholipid bilayer of DOPG and DOPS upon saposin C interaction at acidic pH utilizing ^{31}P and ^{2}H solid-state NMR spectroscopy, *Biochim. Biophys. Acta 1717*, 58−66.
48. Zhang, W. Y., and Smith, S. O. (2005) Mechanism of penetration of Antp(43−58) into membrane bilayers, *Biochemistry 44*, 10110−10118.
49. Sharpe, S., Yau, W. M., and Tycko, R. (2006) Structure and dynamics of the HIV-1 Vpu transmembrane domain revealed by solid-state NMR with magic-angle spinning, *Biochemistry 45*, 918−933.
50. Harada, E., Todokoro, Y., Akutsu, H., and Fujiwara, T. (2006) Detection of peptide-phospholipid interaction sites in bilayer membranes by ^{13}C NMR spectroscopy: Observation of ^{2}H/^{31}P-selective ^{1}H-depolarization under magic-angle spinning, *J. Am. Chem. Soc. 128*, 10654−10655.
51. Toke, O., Maloy, W. L., Kim, S. J., Blazyk, J., and Schaefer, J. (2004) Secondary structure and lipid contact of a peptide antibiotic in phospholipid Bilayers by REDOR, *Biophys. J. 87*, 662−674.
52. Cegelski, L., Rice, C. V., O'Connor, R. D., Caruano, A. L., Tochtrop, G. P., Cai, Z. Y., Covey, D. F., and Schaefer, J. (2005) Mapping the locations of estradiol and potent neuroprotective analogues in phospholipid bilayers by REDOR, *Drug Dev. Res. 66*, 93−102.
53. Matsuoka, S., Ikeuchi, H., Matsumori, N., and Murata, M. (2005) Dominant formation of a single-length channel by amphotericin B in dimyristoylphosphatidylcholine membrane evidenced by ^{13}C-^{13}P rotational echo double resonance, *Biochemistry 44*, 704−710.
54. Aloia, R. C., Tian, H., and Jensen, F. C. (1993) Lipid composition and fluidity of the human immunodeficiency virus envelope and host cell plasma membranes, *Proc. Natl. Acad. Sci. U.S.A. 90*, 5181−5185.
55. Yang, J., Parkanzky, P. D., Bodner, M. L., Duskin, C. G., and Weliky, D. P. (2002) Application of REDOR subtraction for filtered MAS observation of labeled backbone carbons of membrane-bound fusion peptides, *J. Magn. Reson. 159*, 101−110.
56. Wasniewski, C. M., Parkanzky, P. D., Bodner, M. L., and Weliky, D. P. (2004) Solid-state nuclear magnetic resonance studies of HIV and influenza fusion peptide orientations in membrane bilayers using stacked glass plate samples, *Chem. Phys. Lipids 132*, 89−100.
57. Brugger, B., Glass, B., Haberkant, P., Leibrecht, I., Wieland, F. T., and Krasslich, H. G. (2006) The HIV lipidome: A raft with an unusual composition, *Proc. Natl. Acad. Sci. U.S.A. 103*, 2641−2646.
58. Gullion, T., and Schaefer, J. (1989) Rotational-echo double-resonance NMR, *J. Magn. Reson. 81*, 196−200.
59. Yang, J., Prorok, M., Castellino, F. J., and Weliky, D. P. (2004) Oligomeric β-structure of the membrane-bound HIV-1 fusion peptide formed from soluble monomers, *Biophys. J. 87*, 1951−1963.
60. Cevc, G. (1987) How membrane chain melting properties are regulated by the polar surface of the lipid bilayer, *Biochemistry 26*, 6305−6310.
61. Macosko, J. C., Kim, C. H., and Shin, Y. K. (1997) The membrane topology of the fusion peptide region of influenza hemagglutinin determined by spin-labeling EPR, *J. Mol. Biol. 267*, 1139−1148.
62. Han, X., Bushweller, J. H., Cafiso, D. S., and Tamm, L. K. (2001) Membrane structure and fusion-triggering conformational change of the fusion domain from influenza hemagglutinin, *Nat. Struct. Biol. 8*, 715−720.
63. Afonin, S., Dur, U. H. N., Glaser, R. W., and Ulrich, A. S. (2004) 'Boomerang'-like insertion of a fusogenic peptide in a lipid membrane revealed by solid-state ^{19}F NMR, *Magn. Reson. Chem. 42*, 195−203.
64. Yang, J., Parkanzky, P. D., Khunte, B. A., Canlas, C. G., Yang, R., Gabrys, C. M., and Weliky, D. P. (2001) Solid state NMR measurements of conformation and conformational distributions in the membrane-bound HIV-1 fusion peptide, *J. Mol. Graphics Modell. 19*, 129−135.
65. Morcombe, C. R., and Zilm, K. W. (2003) Chemical shift referencing in MAS solid state NMR, *J. Magn. Reson. 162*, 479−486.
66. Zhang, H. Y., Neal, S., and Wishart, D. S. (2003) RefDB: A database of uniformly referenced protein chemical shifts, *J. Biomol. NMR 25*, 173−195.
67. Igumenova, T. I., Wand, A. J., and McDermott, A. E. (2004) Assignment of the backbone resonances for microcrystalline ubiquitin, *J. Am. Chem. Soc. 126*, 5323−5331.
68. Franks, W. T., Zhou, D. H., Wylie, B. J., Money, B. G., Graesser, D. T., Frericks, H. L., Sahota, G., and Rienstra, C. M. (2005) Magic-angle spinning solid-state NMR spectroscopy of the β1 immunoglobulin binding domain of protein G (GB1): ^{15}N and ^{13}C chemical shift assignments and conformational analysis, *J. Am. Chem. Soc. 127*, 12291−12305.
69. Marulanda, D., Tasayco, M. L., Cataldi, M., Arriaran, V., and Polenova, T. (2005) Resonance assignments and secondary structure analysis of *E. coli* thioredoxin by magic angle spinning solid-state NMR spectroscopy, *J. Phys. Chem. B 109*, 18135−18145.
70. Bodner, M. L., Gabrys, C. M., Parkanzky, P. D., Yang, J., Duskin, C. A., and Weliky, D. P. (2004) Temperature dependence and resonance assignment of ^{13}C NMR spectra of selectively and uniformly labeled fusion peptides associated with membranes, *Magn. Reson. Chem. 42*, 187−194.

71. Bloom, M., Evans, E., and Mouritsen, O. G. (1991) Physical properties of the fluid lipid-bilayer component of cell membranes: A perspective, *Q. Rev. Biophys. 24*, 293−397.
72. Gabrys, C. M., Yang, J., and Weliky, D. P. (2003) Analysis of local conformation of membrane-bound and polycrystalline peptides by two-dimensional slow-spinning rotor-synchronized MAS exchange spectroscopy, *J. Biomol. NMR 26*, 49−68.
73. McDowell, L. M., Holl, S. M., Qian, S. J., Li, E., and Schaefer, J. (1993) Inter-tryptophan distances in rat cellular retinol-binding Protein II by solid-state NMR, *Biochemistry 32*, 4560−4563.
74. Anderson, R. C., Gullion, T., Joers, J. M., Shapiro, M., Villhauer, E. B., and Weber, H. P. (1995) Conformation of [1-^{13}C,^{15}N]acetyl-L-carnitine. Rotational-echo, double-resonance nuclear magnetic resonance spectroscopy, *J. Am. Chem. Soc. 117*, 10546−10550.
75. Gullion, T. (1998) Introduction to rotational-echo, double-resonance NMR, *Concepts Magn. Reson. 10*, 277−289.
76. Bennett, A. E., Rienstra, C. M., Auger, M., Lakshmi, K. V., and Griffin, R. G. (1995) Heteronuclear decoupling in rotating solids, *J. Chem. Phys. 103*, 6951−6958.
77. Bevington, P. R., and Robinson, D. K. (1992) *Data Reduction and Error Analysis for the Physical Sciences*, 2nd ed., McGraw-Hill, Boston.
78. Mueller, K. T. (1995) Analytic solutions for the time evolution of dipolar-dephasing NMR signals, *J. Magn. Reson., Ser. A 113*, 81−93.
79. Raghunathan, V., Gibson, J. M., Goobes, G., Popham, J. M., Louie, E. A., Stayton, P. S., and Drobny, G. P. (2006) Homonuclear and heteronuclear NMR studies of a statherin fragment bound to hydroxyapatite crystals, *J. Phys. Chem. B 110*, 9324−9332.
80. Pearson, R. H., and Pascher, I. (1979) Molecular structure of lecithin dihydrate, *Nature 281*, 499−501.
81. Pascher, I., Sundell, S., Harlos, K., and Eibl, H. (1987) Conformation and packing properties of membrane lipids: The crystal structure of sodium dimyristoylphosphatidylglycerol, *Biochim. Biophys. Acta 896*, 77−88.
82. Venable, R. M., Brooks, B. R., and Pastor, R. W. (2000) Molecular dynamics simulations of gel ($L_{\beta 1}$) phase lipid bilayers in constant pressure and constant surface area ensembles, *J. Chem. Phys. 112*, 4822−4832.
83. Bennett, A. E., Ok, J. H., Griffin, R. G., and Vega, S. (1992) Chemical-shift correlation spectroscopy in rotating solids: Radio frequency-driven dipolar recoupling and longitudinal exchange, *J. Chem. Phys. 96*, 8624−8627.
84. Gullion, T., and Vega, S. (1992) A simple magic angle spinning NMR experiment for the dephasing of rotational echoes of dipolar coupled homonuclear spin pairs, *Chem. Phys. Lett. 194*, 423−428.
85. Gordon, L. M., Mobley, P. W., Pilpa, R., Sherman, M. A., and Waring, A. J. (2002) Conformational mapping of the N-terminal peptide of HIV-1 gp41 in membrane environments using ^{13}C-enhanced Fourier transform infrared spectroscopy, *Biochim. Biophys. Acta 1559*, 96−120.
86. Castano, S., and Desbat, B. (2005) Structure and orientation study of fusion peptide FP23 of gp41 from HIV-1 alone or inserted into various lipid membrane models (mono-, bi- and multibi-layers) by FT-IR spectroscopies and Brewster angle microscopy, *Biochim. Biophys. Acta 1715*, 81−95.
87. Sackett, K., and Shai, Y. (2005) The HIV fusion peptide adopts intermolecular parallel β-sheet structure in membranes when stabilized by the adjacent N-terminal heptad repeat: A ^{13}C FTIR study, *J. Mol. Biol. 350*, 790−805.
88. Chan, D. C., Fass, D., Berger, J. M., and Kim, P. S. (1997) Core structure of gp41 from the HIV envelope glycoprotein, *Cell 89*, 263−273.
89. Weissenhorn, W., Dessen, A., Harrison, S. C., Skehel, J. J., and Wiley, D. C. (1997) Atomic structure of the ectodomain from HIV-1 gp41, *Nature 387*, 426−430.
90. Tan, K., Liu, J., Wang, J., Shen, S., and Lu, M. (1997) Atomic structure of a thermostable subdomain of HIV-1 gp41, *Proc. Natl. Acad. Sci. U.S.A. 94*, 12303−12308.
91. Caffrey, M., Cai, M., Kaufman, J., Stahl, S. J., Wingfield, P. T., Covell, D. G., Gronenborn, A. M., and Clore, G. M. (1998) Three-dimensional solution structure of the 44 kDa ectodomain of SIV gp41, *EMBO J. 17*, 4572−4584.
92. Yang, Z. N., Mueser, T. C., Kaufman, J., Stahl, S. J., Wingfield, P. T., and Hyde, C. C. (1999) The crystal structure of the SIV gp41 ectodomain at 1.47 Å resolution, *J. Struct. Biol. 126*, 131−144.
93. Modis, Y., Ogata, S., Clements, D., and Harrison, S. C. (2004) Structure of the dengue virus envelope protein after membrane fusion, *Nature 427*, 313−319.
94. Gibbons, D. L., Vaney, M. C., Roussel, A., Vigouroux, A., Reilly, B., Lepault, J., Kielian, M., and Rey, F. A. (2004) Conformational change and protein protein interactions of the fusion protein of Semliki Forest virus, *Nature 427*, 320−325.
95. Roche, S., Bressanelli, S., Rey, F. A., and Gaudin, Y. (2006) Crystal structure of the low-pH form of the vesicular stomatitis virus glycoprotein G, *Science 313*, 187−191.
96. Heldwein, E. E., Lou, H., Bender, F. C., Cohen, G. H., Eisenberg, R. J., and Harrison, S. C. (2006) Crystal structure of glycoprotein B from herpes simplex virus 1, *Science 313*, 217−220.
97. Hessa, T., Kim, H., Bihlmaier, K., Lundin, C., Boekel, J., Andersson, H., Nilsson, I., White, S. H., and von Heijne, G. (2005) Recognition of transmembrane helices by the endoplasmic reticulum translocon, *Nature 433*, 377−381.
98. Charloteaux, B., Lorin, A., Crowet, J. M., Stroobant, V., Lins, L., Thomas, A., and Brasseur, R. (2006) The N-terminal 12 residue long peptide of HIV gp41 is the minimal peptide sufficient to induce significant T-cell-like membrane destabilization in vitro, *J. Mol. Biol. 359*, 597−609.
99. Smaby, J. M., Brockman, H. L., and Brown, R. E. (1994) Cholesterol's interfacial interactions with sphingomyelins and phosphatidylcholines: Hydrocarbon chain structure determines the magnitude of condensation, *Biochemistry 33*, 9135−9142.
100. Tristram-Nagle, S., Liu, Y. F., Legleiter, J., and Nagle, J. F. (2002) Structure of gel phase DMPC determined by X-ray diffraction, *Biophys. J. 83*, 3324−3335.

BI6024808

This supporting information demonstrates the derivation of $(\Delta S/S_0)^{lab}$ for the HFP2-^{14}AAG samples. The $(\Delta S/S_0)^{lab}$ refers to the signals expected from the ^{14}AAG ^{13}COs and is calculated by removing natural abundance (*na*) ^{13}CO contributions from $(\Delta S/S_0)^{exp}$:

$$\left(\frac{\Delta S}{S_0}\right)^{exp} = \frac{S_0^{lab} + S_0^{na} - S_1^{lab} - S_1^{na}}{S_0^{lab} + S_0^{na}} = 1 - \frac{S_1^{lab}}{S_0^{lab} + S_0^{na}} - \frac{S_1^{na}}{S_0^{lab} + S_0^{na}} \quad (1)$$

Multiplication of the far-left and far-right sides of Eq. 1 by $(S_0^{lab} + S_0^{na})/S_0^{lab}$ is followed by algebraic manipulation:

$$\left[\left(1 + \frac{S_0^{na}}{S_0^{lab}}\right) \times \left(\frac{\Delta S}{S_0}\right)^{exp}\right] = \left(\frac{\Delta S}{S_0}\right)^{lab} + \frac{\left(\Delta S^{na}\right)}{S_0^{lab}} \quad (2)$$

Multiplication of the far-right term by (S_0^{na}/S_0^{na}) is followed by algebraic manipulation to yield Eq. 2 from the main text:

$$\left(\frac{\Delta S}{S_0}\right)^{lab} = \left[\left(1 + \frac{S_0^{na}}{S_0^{lab}}\right) \times \left(\frac{\Delta S}{S_0}\right)^{exp}\right] - \left[\left(\frac{S_0^{na}}{S_0^{lab}}\right) \times \left(\frac{\Delta S}{S_0}\right)^{na}\right] \quad (3)$$

(S_0^{na}/S_0^{lab}) was calculated from the numbers of natural abundance and labeled ^{13}COs in HFP2-^{14}AAG and $(\Delta S/S_0)^{na}$ was calculated as the average of $(\Delta S/S_0)^{exp}$ for the HFP2-^{5}GAL, HFP3-^{8}FLG, and HFP2-^{11}FLG samples. Although the latter calculation is an approximation, uncertainties in $(\Delta S/S_0)^{na}$ have a relatively small impact on the uncertainty of $(\Delta S/S_0)^{lab}$. For example, consider the spectra for the PC:PG samples at $\tau = 24$ ms. The values of (S_0^{na}/S_0^{lab}), $(\Delta S/S_0)^{exp}$, and $(\Delta S/S_0)^{na}$ are 0.084, 0.419 ± 0.014, and 0.134, respectively, and result in $(\Delta S/S_0)^{lab} = 0.443 \pm 0.015$. If $(\Delta S/S_0)^{na}$ were 0.0 or 0.25, $(\Delta S/S_0)^{lab}$ would be 0.454 or 0.433 which are within the reported experimental uncertainty of $(\Delta S/S_0)^{lab}$.